

# The effect of surface geometry on collisions between nanoparticles

Yoichi Takato<sup>a,b,\*</sup>, Michael E. Benson<sup>a</sup>, Surajit Sen<sup>a,\*\*</sup>

<sup>a</sup>*Department of Physics*

*The State University of New York at Buffalo, Buffalo, New York 14260-1500, USA*

<sup>b</sup>*Mathematical Soft Matter Unit*

*Okinawa Institute of Science and Technology Graduate University, Onna-son, Okinawa, 904-0495 Japan*

---

## Abstract

In this molecular dynamics study, we examine the local surface geometric effects of the normal impact force between two approximately spherical nanoparticles that collide in a vacuum. Three types of surface geometries, facets, sharp crystal edges, and amorphous surfaces of nanoparticles with radii  $R < 10$  nm are considered, and the impact force is compared with its macroscopic counterpart described by a nonlinear contact force,  $F_N \propto \delta^n$  with  $n = 3/2$  derived by Hertz (1881), where  $\delta$  is the overlap induced by elastic compression. We study the surface geometry-dependent impact force. For facet-facet impact, the mutual contact surface area does not expand due to the large facet surface, and this in turn leads to a non-Hertz impact force,  $n < 3/2$ . A Hertz-like contact force,  $n \approx 3/2$ , is recovered in the edge contact and in the amorphous surface contact, allowing expansion of the mutual contact surface area. The results suggest that collisions of amorphous nanoparticles or nanoparticles with sharp edges may maintain dynamic phenomena, such as breathers and solitary waves, originating from the nonlinear contact force.

**Keywords:** Contact force, Nanoparticle, Collision, Surface roughness

**PACS:** 46.55.+d, 45.50.Tn, 61.46.Df, 05.45.-a

---

## 1. Introduction

The discrete nature of nanoscale materials has often revealed surprising phenomena. Nanoscale normal contact force and friction laws depend strongly on the contact. A molecular dynamics (MD) study by Luan and Robbins [1] demonstrated the breakdown of continuum theory in a system of nanoscale non-adhesive cylinders made to model contact between substrates and atomic force microscope tips. The normal contact force for rough surfaces of solids with amorphous and crystal structures revealed significant departures from the Hertz contact force for contacting elastic perfect spheres [2]. Atomically rough surfaces on contacting objects influence the contact considerably, and local surface geometry in the vicinity of the contact region promotes variations of the contact surface area [1, 3].

Atomic surface asperities also dictate impact phenomena in nanoparticles. Gold nanoparticles can take a near-spherical shape, one of the thermodynamically stable shapes [4], and the surface of such a nanoparticle is comprised of crystal steps and terraces. Facets and crystal steps in small nanoparticles can make them “rough”, which in turn affects the nature of their interactions. The lack of spherical nanoparticle symmetry often leads to more complex dynamics than the Hertz contact theory for perfect spheres. Roll, slide, and deflection of colliding nanoparticles arising from shape asymmetry have been observed elsewhere [5, 6].

In dynamics, the coefficient of restitution often suffices to predict overall behavior of a dissipative many-body system such as clustering of dissipative particles [7]. Precise measurement of impact force, however, is critical for certain dynamic systems. A recent MD simulation demonstrated that a one-dimensional chain of nanoscale buckyballs can permit the propagation of a solitary wave [8], which is a non-dispersive propagating wave in a macroscopic

---

\*Corresponding author

\*\*Principal corresponding author

Email addresses: ytakato@buffalo.edu (Yoichi Takato), mebenso@buffalo.edu (Michael E. Benson), sen@buffalo.edu (Surajit Sen)

granular system discovered by Nesterenko [9]. Realization of the solitary wave at nanoscale implies that the interaction between buckyballs is described by a nonlinear force. That is, the power of overlap must satisfy  $n > 1$  so that a sharp propagating pulse of energy can be formed [10, 11].

Direct observation of the impact force of repulsive nanoparticles made by MD simulations, on the other hand, has been reported in a few papers [12, 13]. The nature of impact forces between rough surfaces of colliding nanoparticles is not fully understood yet. Our MD study presents precise details of contact forces for collisions between nanoparticles having three different contact surface geometries, in order to investigate the influence of surface roughness in a systematic fashion. The surface of an amorphous nanoparticle and two surface geometries, facets and sharp crystal edges of a face-centered cubic (fcc) crystal nanoparticle, are considered as contact surfaces.

Many MD studies on nanoparticle collisions indicate that nanoparticles are highly elastic if the impact velocity is kept below their material yield point, although a small amount of the initial kinetic energy admittedly dissipates during the impact process [12, 14, 15, 16]. In addition, a recent study showed that the effect of nanoparticle adhesive property is negligibly small [17] if the adhesive nanoparticles collide beyond a critical velocity determined by the balance between adhesion and elastic energies [18, 19, 6, 20]. Therefore, for simplicity, we consider only repulsive nanoparticles in our simulation, adopting the Weeks-Chandler-Andersen (WCA) potential [21, 1, 16], which is a type of Lennard-Jones (LJ) potential modified to yield a purely repulsive interaction.

In our work, a non-Hertzian contact force exhibiting velocity dependence is found in monocrystalline nanoparticles impacting on facets. This type of impact makes the dynamics of a collision considerably different from Hertzian contact mechanics. For instance, the mutual contact surface created between two nanoparticles in contact remains unchanged, as opposed to the evolving contact surface area of a Hertzian sphere. In contrast, the Hertzian contact force is a good approximation for crystalline nanoparticles impacting on sharp crystal step edges. Furthermore, amorphous nanoparticles with relatively smooth surfaces and substantially spherical shapes yield an impact force that resembles the Hertzian contact force.

The present work is organized as follows: the Hertz contact theory is briefly reviewed in Sec. 2. Sec. 3 discusses our nanoparticle models and computational methods. Contact forces for colliding nanoparticles made from amorphous and crystal structures are displayed in Sec. 4.1. Furthermore, the maximum contact area and maximum compression for facet contact for monocrystalline nanoparticles are compared with those for Hertzian spheres in Sec. 4.2. In Sec. 5, a departure is discussed. The conclusions are presented in Sec. 6.

## 2. Hertz contact theory

Hertz derived a normal compressive force  $F_H$  between two statically contacting elastic spheres that have smooth surfaces [2, 22]. The force is expressed in terms of overlap  $\delta = (2R - d)/2$  for two identical spheres of diameter  $2R$  and center-to-center intersphere distance  $d$  under compression,

$$F_H = \kappa_H \delta^n, \quad (1)$$

where  $n = 3/2$  and  $\kappa_H = (4/3)E^*R^{1/2}$ . The reduced Young's modulus is  $E^* = E/[2(1 - \nu^2)]$  with Young's modulus  $E$  and Poisson ratio  $\nu$ . The reduced radius is  $R^* = R/2$  for identical spheres of radius  $R$ . The contact force grows nonlinearly with increasing overlap. The underlying mechanism that yields the nonlinearity is the varying mutual contact surface area between the spheres as a function of compression. The shape of the contact surface in the theory is assumed to be a circle with radius  $a_H$ , from which its area is  $\pi a_H^2$ . General contact surface shapes and their resultant contact forces including Hertzian force are discussed in Ref. [23]. The geometrical relation between the displacement and the contact area under compression gives

$$a_H = \sqrt{R^* \delta}. \quad (2)$$

Hence, the contact area expands in proportion to the square root  $\sqrt{\delta}$  of the overlap.

The equations are derived under static compression. For colliding elastic spheres that are assumed to follow the Hertz contact theory by ignoring energy dissipation via surface vibrations, there are several important quantities that characterize the spheres. A maximum overlap  $\delta_H^{\max}$  is the overlap when the colliding spheres instantaneously come to rest during a collision. Maximum overlap takes the highest value when the initial kinetic energy associated with

the relative velocity  $v_{\text{imp}}$  is fully converted into elastic energy to deform the spheres. The maximum overlap  $\delta_{\text{H}}^{\text{max}}$  is therefore expressed by Eq. (3), taking into account the energy balance between kinetic energy and elastic energy.

$$\delta_{\text{H}}^{\text{max}} = \left( \frac{15}{16} \frac{M^*}{E^* R^{*1/2}} v_{\text{imp}}^2 \right)^{2/5}. \quad (3)$$

The contact radius for the spheres at maximum compression is then obtained from Eqs. (2) and (3),

$$a_{\text{H}}^{\text{max}} = \sqrt{R^* \delta_{\text{H}}^{\text{max}}} = \left( \frac{15}{16} \frac{M^* R^{*2}}{E^*} v_{\text{imp}}^2 \right)^{1/5}. \quad (4)$$

This reveals that the maximum contact radius scales with impact velocity to the 2/5th power.

### 3. Numerical simulations

#### 3.1. Models

For an investigation of the dynamic contact force between colliding nanoparticles, nearly spherical argon nanoparticles  $\xi$  and  $\eta$  of equal radius  $R$  are prepared. To study the influence of surface roughness, we employ crystal and amorphous structures as base materials for making our nanoparticles.

Crystalline nanoparticles are carved out of an fcc single crystal of solid argon. The resultant nanoparticles have atomic roughness such as crystal facets and steps on their exterior surfaces due to their crystal structures (See the insets of Figs. 1(c)–(f).). We take advantage of the presence of the surface roughness to obtain contact forces at particular points on the surfaces. The  $\{001\}$  facets are chosen for studying *facet collisions* and some sharp crystal edges are chosen for studying the *edge collision* problem.

The amorphous structure is obtained by quenching a molten argon block from temperature  $T = 70$  K to 0.02 K at a rate  $8 \times 10^{10}$  K/s [24, 25], followed by equilibrations at  $T_{\text{eq}} = 0.02$  K. A nearly spherical nanoparticle is then created by cutting the block (See the insets of Figs. 1(a)–(b)). Radial distribution functions computed from our equilibrated nanoparticles confirm the amorphous structure [26].

A pure repulsion between two contacting nanoparticles is considered by employing the WCA potential in Eq. (6) as used for our previous study [16] and for the Luan and Robbins's study [1].

#### 3.2. Interatomic potentials

Our nonequilibrium MD simulations here use two interatomic potentials for argon nanoparticles. The shifted 12-6 LJ potential  $V^{\text{LJ}}$  in Eq. (5) describes an interatomic interaction between a pair of atoms  $i$  and  $j$  in either nanoparticle  $\xi$  or nanoparticle  $\eta$ , i.e.,  $i, j \in \xi$  or  $i, j \in \eta$  as follows,

$$V^{\text{LJ}} = \left\{ 4\epsilon \left[ \left( \frac{\sigma}{r_{ij}} \right)^{12} - \left( \frac{\sigma}{r_{ij}} \right)^6 \right] + V(r_c^{\text{LJ}}) \right\} H(r_c^{\text{LJ}} - r_{ij}). \quad (5)$$

The  $r_{ij}$  denotes an interatomic distance between  $i$ -th and  $j$ -th atoms,  $\sigma$  is the distance at which the potential is zero, and  $\epsilon$  is the depth of the potential. The Heaviside step function  $H$  describes a cutoff of the potential at  $r_c^{\text{LJ}} = 2.5\sigma$ . The potential is shifted by  $V(r_c^{\text{LJ}})$  to get rid of a discontinuity at  $r_{ij} = r_c^{\text{LJ}}$  that stems from the adoption of the cutoff.

In addition, the WCA potential  $V^{\text{WCA}}$  in Eq. (6) is adopted to attain purely repulsive nanoparticles by setting its cutoff radius at  $r_c^{\text{WCA}} = 2^{1/6}\sigma$  where the potential is minimal. The use of this cutoff value makes the potential purely repulsive [21]. This potential applies only to a pair of atoms  $p$  and  $q$  belonging to nanoparticle  $\xi$  or nanoparticle  $\eta$ , respectively,

$$V^{\text{WCA}} = \left\{ 4\epsilon \left[ \left( \frac{\sigma}{r_{pq}} \right)^{12} - \left( \frac{\sigma}{r_{pq}} \right)^6 \right] + \epsilon \right\} H(r_c^{\text{WCA}} - r_{pq}). \quad (6)$$

For argon atoms,  $\sigma = 0.3405$  nm and  $\epsilon = 1.654 \times 10^{-21}$  J are set in both potentials.

### 3.3. Computation

Equations of motion for argon atoms are solved by the velocity Verlet algorithm with integration time  $\Delta t = 1.08 \times 10^{-14}$  s for crystalline nanoparticles and  $\Delta t = 4.3 \times 10^{-15}$  s for amorphous nanoparticles.

All the nanoparticles prepared are initially relaxed over sufficient time steps in the canonical (constant-temperature) ensemble at temperature  $T_{\text{eq}} = 0.02$  K. After the relaxation, the nanoparticles are brought into head-on collision at a relative impact velocity  $v_{\text{imp}} = v_{\xi} - v_{\eta}$  in the microcanonical (constant-energy) ensemble. The  $v_{\xi}$  and  $v_{\eta}$  denote the center-of-mass velocities in  $z$ -direction for the nanoparticles  $\xi$  and  $\eta$ , respectively.

Our MD simulations presented hereafter are carried out by LAMMPS [27].

### 3.4. Calculation of impact force

An impact force  $\mathbf{F}_{\xi\eta}$  acting on the mutual contact surfaces formed between two nanoparticles  $\xi$  and  $\eta$  in contact is computed by summing the individual interatomic forces  $\mathbf{f}_{pq}$  for a pair of atoms  $p$  and  $q$  that are positioned in separate nanoparticles  $\xi$  and  $\eta$ , respectively. The expression for the force  $\mathbf{F}_{\xi\eta}$  is given by

$$\mathbf{F}_{\xi\eta} = \sum_{p \in \xi} \sum_{q \in \eta} \mathbf{f}_{pq}. \quad (7)$$

The impact force  $\mathbf{f}_{pq}$  determined by the WCA potential in Eq. (6) leads to a purely compressive impact force  $\mathbf{F}_{\xi\eta}$  that causes deformation of the nanoparticles during a head-on collision.

The normal component  $F_N$  of the impact force  $\mathbf{F}_{\xi\eta}$  is obtained in such a way that  $F_N = \mathbf{F}_{\xi\eta} \cdot \mathbf{d}_{\xi\eta} / |\mathbf{d}_{\xi\eta}|$ , where  $\mathbf{d}_{\xi\eta}$  is the instantaneous center-of-mass distance of the colliding nanoparticles  $\xi$  and  $\eta$  in a direction parallel to a line segment between the centers of the colliding nanoparticles. Although the direction of  $\mathbf{d}_{\xi\eta}$  is initially aligned with the  $z$  axis, thermal vibrations, slip, and rotation that break the reflectional symmetry of the system frequently result in a small deflection of the contacting nanoparticles. The direction of  $\mathbf{d}_{\xi\eta}$  during the collision does not necessarily match the  $z$  axis, accordingly. The normal force  $F_N$  computed by the above-stated definition is used to describe the nanoparticle interactions.

## 4. Simulation Results

We present simulation results in this section for impact phenomena found in our repulsive nanoparticles. Impact forces for amorphous and monocrystalline nanoparticles in facet and edge contacts are shown in Sec. 4.1. Additionally, dynamic behaviors of deformation in the facet contact case are compared in Sec. 4.2 with theoretical predictions for corresponding Hertzian spheres. For visualization of nanoparticles vmd [28] is utilized.

### 4.1. Impact force

Fig. 1 shows normal contact forces for amorphous nanoparticles in (a) and (b), for fcc nanoparticles in edge contact in (c) and (d) and for fcc nanoparticles in facet contact in (e) and (f). Each curve represents a dimensionless normal contact force  $\tilde{F}_N := F_N / E^* R^2$  between contacting nanoparticles at an impact velocity  $v_{\text{imp}}$  plotted as a function of a dimensionless overlap  $\tilde{\delta} := \delta / R$ . The dimensionless normal force and the dimensionless overlap are henceforth termed a force and an overlap, respectively, for the sake of simplicity. Two different radii  $R$  are chosen to see the size dependence of the force. Furthermore, four different impact velocities  $v_{\text{imp}} = 10, 21, 31$ , and  $52$  m/s are selected to analyze a dynamic effect on the force. To see the similarity between the nanoparticles and corresponding elastic perfect spheres, the Hertzian contact force described by Eq. (1) is depicted as a dashed line in each plot.

The force is exhibited only in the loading stage of the collision, which is determined by a point where the overlap  $\tilde{\delta}$  takes its maximum value. Although nanoparticles are highly elastic, unlike elastic bodies in contact, the force in the unloading stage mostly does not follow back the path of the force-overlap curve taken in the loading stage. This is because of irreversible processes. A part of the initial kinetic energy is almost always converted to thermal energy during the collision.

All plots in Fig. 1 have two compression regimes where the rates of change differ noticeably in impact force. In a curve for  $R = 2.5$  nm and  $v_{\text{imp}} = 52$  m/s in Fig. 1(e), for instance, its critical overlap  $\tilde{\delta}_c$  is identified as a kink observed at around  $\tilde{\delta} \sim 10^{-2}$ , which varies depending on the contact type, size, and impact speed. The force below the critical

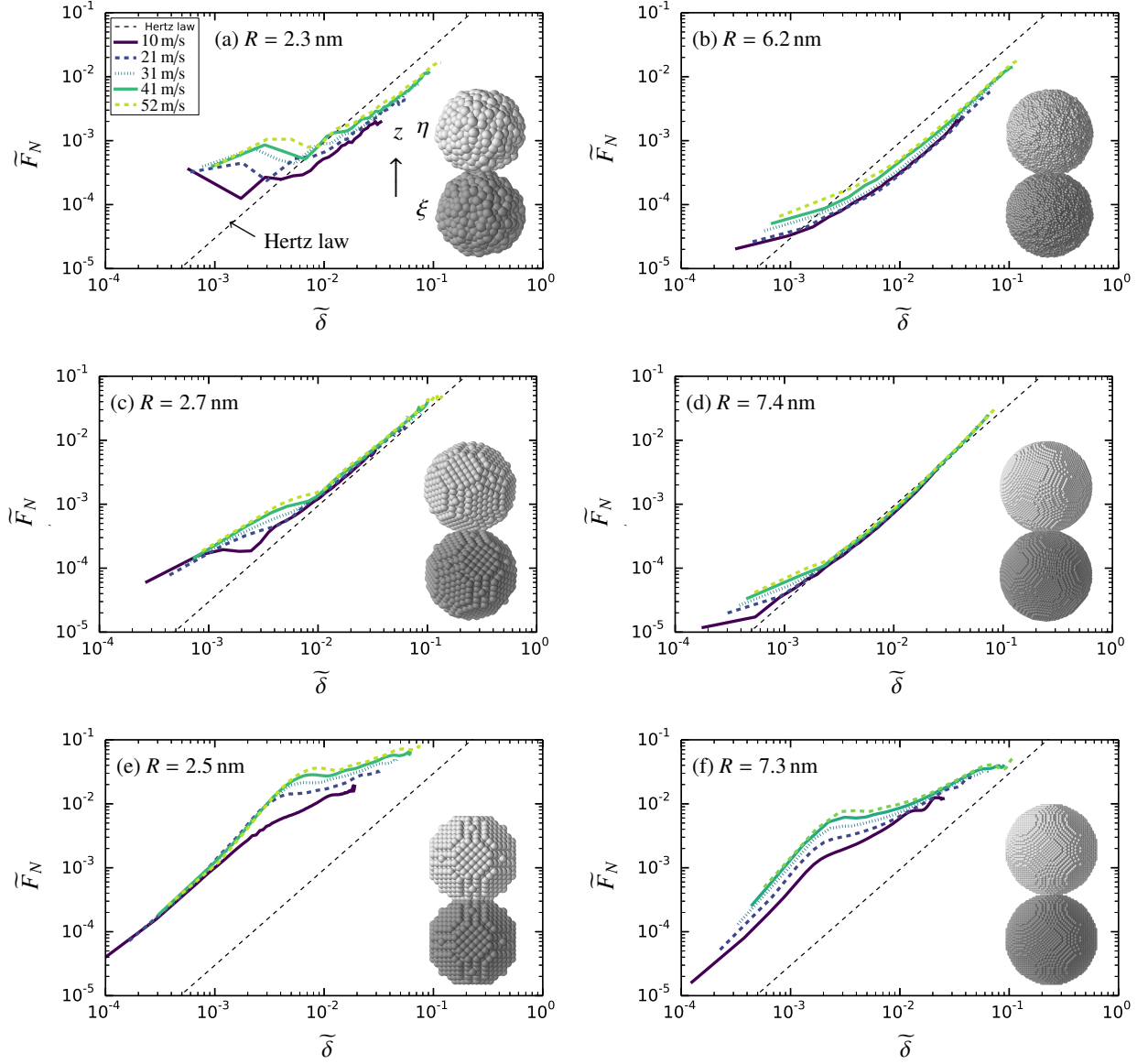


Figure 1: (Color online) Impact force  $\tilde{F}_N$  for contacting nanoparticles of radius  $R$  during the loading stage, plotted as a function of overlap  $\tilde{\delta}$ . The force depicted at each impact velocity  $v_{\text{imp}}$  is a set of piecewise averages over the initial conditions. The dashed line represents the Hertzian force for an fcc crystalline nanoparticle [16]. (a–b) Amorphous nanoparticles in contact. (c–d) Crystalline nanoparticles in edge contact. (e–f) Crystalline nanoparticles in facet contact. The snapshots of nanoparticles shown here are taken at an impact velocity  $v_{\text{imp}} = 21$  m/s.

overlap increases at some constant rate as the overlap increases, and the force above the critical overlap increases further at another rate.

In the high compression regime,  $\tilde{\delta} \gtrsim \tilde{\delta}_c$ , the edge contact in Fig. 1 (c) and (d) shows good agreement with the Hertz contact theory, and the amorphous nanoparticles in Fig. 1 (a) and (b) recover the slope of the Hertz contact force. The facet contact, however, turns out to be distinct from the Hertz contact force in both slope and magnitude.

In the low compression regime,  $\tilde{\delta} \lesssim \tilde{\delta}_c$ , all the forces appear to increase at a rate similar to the Hertz contact force but show large departures in magnitude. The edge contact and amorphous nanoparticles in the same figures possess a gentler mechanical response to impact loads, but the facet contact shows a rapid increase in force in (e) and (f).

Table 1: Impact force for contact surface types and overlap ranges.

	Amorphous nanoparticle	Crystalline nanoparticle	
		Edge contact	Facet contact
Large compression $\tilde{\delta} > \tilde{\delta}_c$	Hertz	Hertz	Non-Hertz
Small compression $\tilde{\delta} < \tilde{\delta}_c$	Non-Hertz	Non-Hertz	Non-Hertz

Impact forces for the aforementioned surface roughnesses and compression levels are summarized in Table 1, and we will show more details in the contact types separately.

#### 4.1.1. Impact between amorphous nanoparticles

The exteriors of the amorphous nanoparticles in Figs. 1(a) and (b) look more spherical than those of the crystalline nanoparticles in Figs. 1(a) and (b). Although individual atoms randomly stacked on the surface form a small asperity, the arrays of atomic steps and associated sharp edges seen in the crystalline nanoparticles are absent due to the disordered arrangement. The facet-free nanoparticle is therefore expected to recover a Hertzian-like force curve with the  $3/2$  power of overlap.

Impact forces  $\tilde{F}_N$  of the large amorphous nanoparticles in Fig. 1 (b) at high compression  $\tilde{\delta} \gtrsim \tilde{\delta}_c$  resemble the Hertz contact force in the sense that  $\tilde{F}_N$  grows with overlap nonlinearly at a rate  $\sim 1.5$  though there is a dynamic effect, that is, the forces increase at a certain overlap fixed as impact velocity increases. The nanoparticles in the inset of Fig. 1(b) have a flat contact surface developed during the collision. The expanding contact surface area seems consistent with the result in Ref. [29], which reported an expanding contact surface area of colliding polymer nanoparticles having a relatively smooth surface like our amorphous nanoparticles. This area is in agreement with that of corresponding Hertz spheres in Eq. (2) when the compression is high enough. This contact surface expansion induced by compression as expressed in Eq. (2) is critical to recover the Hertzian contact force.

The smaller amorphous nanoparticles in Fig. 1(a) show an impact response similar to that of the large ones, but some noise is present. The contact surface of the small nanoparticles in compression involves only a small number of atoms due to their size,  $R = 2.3$  nm, the smallest among our nanoparticles.

#### 4.1.2. Impact on sharp crystal edges

We consider cases where two monocrystalline nanoparticles collide such that they first come into contact on at least one sharp edge on either of the nanoparticles. Fig. 1(c) and (d) illustrate the collisions for fully compressed nanoparticles that are randomly oriented before collision. As noticed, the edge collision case obviously has a contact area smaller than the  $\{001\}$  facet displayed in Fig. 1(e). This allows the contact surface area in edge contact to expand as the overlap increases.

This contact force is in excellent agreement with the Hertz contact force, as shown in Figs. 1(c) and (d). The impact force is well aligned with the Hertzian force when both the nanoparticles are compressed sufficiently,  $\tilde{\delta} > \tilde{\delta}_c$ . In this regime, the magnitude of the impact force has almost negligible velocity dependence. Regardless of the impact velocity variation between 10 and 52 m/s, the forces for the given velocities are all the same up to their maximum overlaps, which now depend on the impact velocity.

#### 4.1.3. Impact on crystal facets

The contact surface for the facet contact in the inset of Fig. 1(e) is obviously distinct from those in the edge contact and amorphous nanoparticle cases. The presence of large surfaces on crystalline nanoparticles and the impact on the facets completely alter the dynamic response of the colliding nanoparticles. Consequently, the impact force between the nanoparticles has a behavior unlike the Hertz contact force in Eq. (1).

When compression of the nanoparticles is low  $\tilde{\delta} < \tilde{\delta}_c$ , all impact forces  $\tilde{F}_N$  at various velocities in Fig. 1(e) are the same, and are considerably higher than their corresponding Hertzian forces. Each force then increases at a lower rate as the compression increases further. The slope of the force-overlap curve in the large overlap region,  $\tilde{\delta} > \tilde{\delta}_c$ , is notably lower than  $n = 3/2$  for the Hertz contact force, shown as a dashed line in Figs. 1(a–e). Furthermore, the force in the same overlap range has a relatively strong velocity dependence, and faster nanoparticles experience stronger repulsive forces.

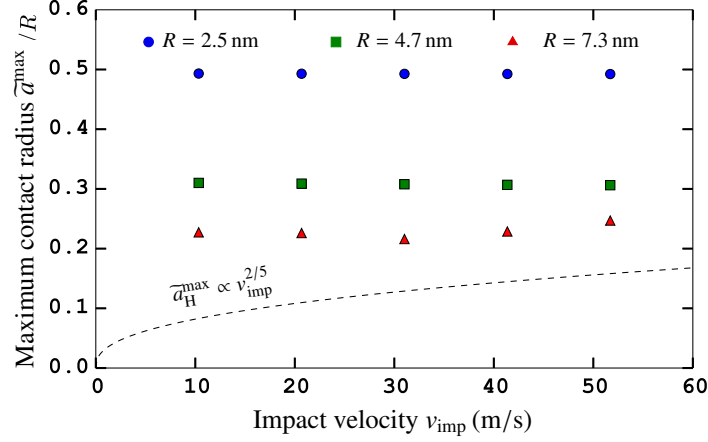


Figure 2: (Color online) The dimensionless maximum contact radius  $\tilde{a}^{\max}$  computed from our simulation data remains constant over the quasi-elastic collision range. The dashed line is predicted by the Hertz contact theory, which is independent of size  $R$ .

The larger nanoparticles in Fig. 1(f) behave qualitatively in the same way as seen in the smaller nanoparticles, that is, the impact force has a higher rate of change at  $\tilde{\delta} < \tilde{\delta}_c$  and a lower rate at  $\tilde{\delta} > \tilde{\delta}_c$ . Large nanoparticles are expected to approach Hertz spheres since as nanoparticle size is increased, the facet area progressively becomes smaller and the role of the facet would vanish in the limiting case of  $R \rightarrow \infty$ . However, these nanoparticles of  $R = 7.3$  nm bear no semblance of Hertzian spheres.

#### 4.2. Dynamic behaviors for facet contact

##### 4.2.1. Contact surface area

The contact surface area developed for Hertzian spheres under compression is described by Eq. (2) and it gives rise to nonlinearity in its mechanical response. In the case of the facet collision, the  $\{001\}$  facets are chosen for surfaces to be contacted, and the facet contact resulted in the non-Hertzian force, as already seen. Thus, it is interesting to see how the mutual contact surface evolves as the nanoparticles are compressed. The contact surface area for nanoparticles of several sizes is examined and compared with the Hertzian sphere case.

Fig. 1(e) shows a representative snapshot for faceted nanoparticles with their  $\{001\}$  facets in contact at maximum compression, and their colliding surfaces possess relatively flat square-like areas. We adopt a new measure to quantify a contact radius  $a$  for our nanoparticles in place of a contact surface area. The contact radius  $a$  is an effective radius for an actual contact surface area that equals a circular surface area  $\pi a^2$ . The actual contact surface of the contacting nanoparticles is not a circle; however, it is convenient to regard the square-like contact surface as a circular surface of radius  $a$  when compared to the radius of the mutual contact surface area formed between the Hertzian spheres. The contact radius  $a$  for nanoparticles is computed by [30]

$$a^2 = \frac{1}{N_s^2} \sum_{i=1}^{N_s} \sum_{j=1}^{N_s} \left[ (x_i - x_j)^2 + (y_i - y_j)^2 \right], \quad (8)$$

where  $x_i$  ( $y_i$ ) and  $x_j$  ( $y_j$ ) are the  $x$  ( $y$ ) component of  $i$ -th and  $j$ -th atom coordinates on the same contact surface, respectively.  $N_s$  denotes the total number of atoms involved in contact.

The nondimensionalized contact radii  $\tilde{a} := a/R$  of three different sized nanoparticles computed by Eq. (8) at their maximum compression are plotted against the impact velocity in Fig. 2.

The plateaus in the figure clearly indicate that the maximum contact radii  $\tilde{a}^{\max}$  remain unchanged. In other words, the facet contact does not allow a contact surface expansion no matter how forcefully the nanoparticles collide, provided that the impact occurs within the range of the quasi-elastic collision regime. Facet sizes are nearly comparable to the radii of small nanoparticles. In particular, the contact radius for the  $R = 2.5$  nm nanoparticle reaches 50% of its radius. By contrast, the surface area for Hertzian spheres expands with increasing impact velocity depicted by a dashed line based on Eq. (2), as seen in Fig. 2.

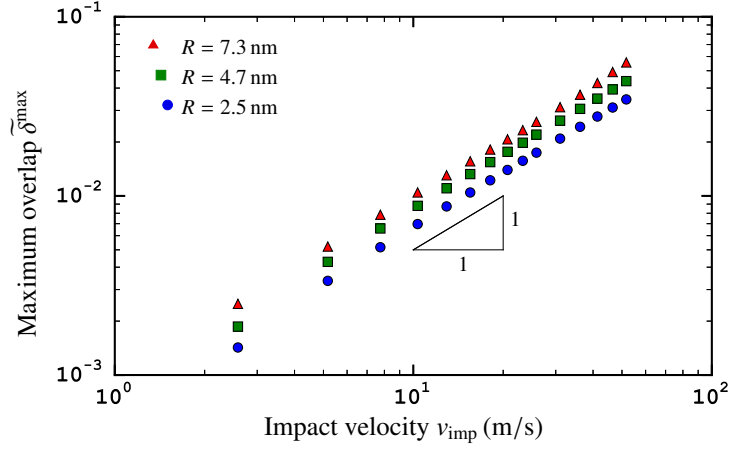


Figure 3: (Color online) The dimensionless maximum overlap  $\tilde{\delta}^{\max}$  obtained from our simulations is proportional to  $v_{\text{imp}}$ . The Hertz contact theory predicts a velocity dependence in  $\tilde{\delta}^{\max} \propto v_{\text{imp}}^{4/5}$ .

#### 4.2.2. Compression

Another mechanical property examined here is how much the nanoparticles are compressed at maximal contact. Colliding elastic spheres show a velocity dependence on the dimensionless maximum overlap  $\tilde{\delta}^{\max} \propto v_{\text{imp}}^{\alpha}$ , where  $\alpha = 4/5$  for the Hertz, but no size dependence according to Eq. (3). The exponent  $\alpha = 4/5$  of the impact velocity  $v_{\text{imp}}$  equals the ratio of the exponent, 2, of the impact velocity in kinetic energy  $(1/2)M^*v_{\text{imp}}^2$  to the exponent  $n + 1 = 5/2$  of the overlap in elastic energy  $\kappa_H \tilde{\delta}^{n+1}$  stored in the deformed Hertzian spheres, i.e.,  $\alpha = 2/(n + 1) = 4/5$ . A different value of the exponent  $\alpha$  in the facet contact case would be anticipated since its force does not obey the Hertzian force in Figs. 1(e) and (f) and the power of the force law,  $n$ , is likely different from  $3/2$ .

Fig. 3 presents the maximum overlap  $\tilde{\delta}^{\max}$  of the nanoparticles. The obtained maximum overlap for three nanoparticle sizes has a size dependence, and the smaller nanoparticles are less deformable. The maximum overlap of the nanoparticles exhibits a velocity dependence and appears to be proportional to the impact velocity. This result differs from the  $4/5$  power of the velocity that the Hertz contact theory yields. This deviation in the exponent demonstrates further evidence of the non-Hertzian contact force observed in the facet contact.

## 5. Discussion

### 5.1. Critical overlap and contact surface area at low compression

We defined the critical overlap  $\tilde{\delta}_c$  as an overlap where the dynamic response of the colliding nanoparticles undergoes a sudden change in slope of a force-overlap curve. This value can reduce the somewhat complex force behavior into two regimes in which the forces grow at different rates in a comparatively smooth manner. It then raises questions about what makes such a change in force at a particular overlap and what influences force behaviors above and below the critical overlap.

Fig. 4(a) is a force-overlap plot for facet contact. In addition, the number  $N_s$  of atoms involved in contact is also included in the plot in order to see how evolution of the contact surface influences the force. The dimensionless impact force  $\tilde{F}_N$  and number  $N_s$  in the plot are obtained by averaging over different initial conditions.

The number  $N_s$  of atoms in contact rises and then saturates as the overlap increases. At saturation, all atoms residing on the very first atomic layer of the facet participate in contact. The atomic layers are stacked in the  $[001]$  direction, and the atoms in the second layer are clearly visible from the exteriors of the nanoparticles in Fig. 1(e). Nevertheless, the second layers never come into contact with the other nanoparticle; hence, further growth of the contact area does not occur.

The kink in the number where contact area growth ends, coincides with the transition of the force behavior at the critical overlap  $\tilde{\delta}_c$ . For the small nanoparticle of  $R = 2.5$  nm the kink is identified at  $\tilde{\delta} \sim 5 \times 10^{-3}$  in Fig. 4(a). Thus,



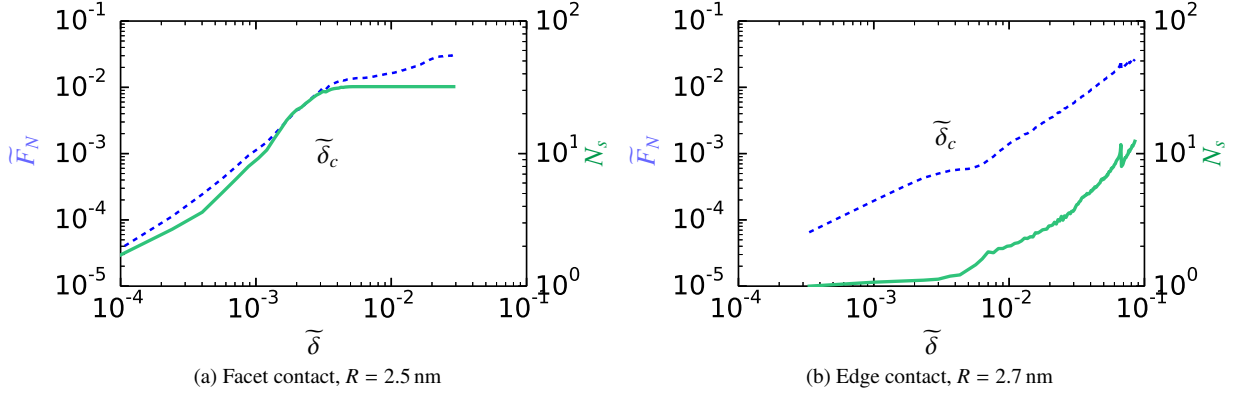


Figure 4: (Color online) The number  $N_s$  of atoms in contact (solid line) and the dimensionless impact force  $\tilde{F}_N$  (dashed line) for faceted nanoparticles that undergo facet contact in (a) or edge contact in (b). Both nanoparticles collide at  $v_{\text{imp}} = 41$  m/s.

we conclude that the critical overlap  $\tilde{\delta}_c$  is the onset of completion of contact of the first atomic layer of the facet, and that no further growth of the area occurs at  $\tilde{\delta} > \tilde{\delta}_c$ .

The constant contact areas presented at  $\tilde{\delta} > \tilde{\delta}_c$  differ from the results for nanoparticles having a facet-free surface in Refs. [30, 31, 32, 33] and in our amorphous nanoparticles and edge contacts. The nanoparticles reported in the articles are crystalline nanoparticles with nearly spherical shapes. They have relatively smooth surfaces, although atomic asperity exists. Contact surface areas expand as the nanoparticles get compressed and follow either the Hertz contact theory or the Johnson-Kendall-Roberts theory [34], in which surface adhesion is incorporated.

At low compression  $\tilde{\delta} < \tilde{\delta}_c$ , where partial contact of the facet occurs, the rising rate of the contact force with increasing overlap is higher. The number  $N_s$  of contacting atoms in this compression domain rises steadily and quickly in a very narrow range of overlap. The dynamic response triggered by the impact load then becomes sharper than that at the higher compression,  $\tilde{\delta} > \tilde{\delta}_c$ .

In the edge contact case, on the other hand, Fig. 4(b), the very low  $N_s$  at  $\tilde{\delta} < \tilde{\delta}_c$  shows that only one atom is involved in contact. The  $N_s$  then increases gradually, which commences in the vicinity of the critical overlap. This means that the nanoparticles are in contact via only a single atom at the very early stage of contact, and for a longer period of contact compared to the facet contact case. The slower compression process happening in a very limited area on the surface is presumably a primary reason that the contact force at  $\tilde{\delta} < \tilde{\delta}_c$  increases more slowly by comparison to that at  $\tilde{\delta} > \tilde{\delta}_c$ .

## 5.2. Hertzian or non-Hertzian?

The failure of the Hertz contact law for facet contact in our crystalline nanoparticles at high compression seems to be attributable to the occurrence of an impact on a large contact area. Since the forces for edge contact and amorphous surface contact shown earlier recover at least the slope of the Hertzian contact force, for sufficient compression. Two past papers may give us another perspective on repulsive nanoparticles in contact.

In an MD-based nanoindentation study [35], the contact force of a small copper nanoparticle of radius  $R = 10$  nm under uniaxial compression in its {001} facets by two opposing rigid plates behaves according to the Hertzian model. The copper atoms in the simulation were modeled by the Embedded Atom Model (EAM) [36] and the pure repulsion between the plates and the copper nanoparticle adopted a harmonic potential.

Moreover, in Ref. [12] a facet collision for two LJ nanoparticles with a pure repulsion acting between the nanoparticles described by a soft potential  $4\epsilon(\sigma/r_{ij})^{12}$  with a cutoff  $2.5\sigma$ , which is the repulsive term in the 12-6 LJ potential, was reported. Its force on the contact surface turned out to be consistent with Hertzian contact theory.

In both papers, the (100) facet on fcc nanoparticles was chosen for contact. The results are inconsistent with our results for facet contact. This discrepancy perhaps arises from the choices in surface interactions, the softer interactions employed in the above papers and the stiffer interaction, i.e. the WCA potential, used in our simulation. Further investigation using different potentials is needed to identify the disagreement.

## 6. Conclusions

We have presented the quasi-elastic interactions of two approximate spherical nanoparticles that undergo a head-on collision obtained by means of non-equilibrium MD simulation. The pure repulsive impact force between two nanoparticles in contact was achieved by adopting the Weeks-Chandler-Andersen potential. To study the effect of atomic scale surface roughness and structure on the impact force, monocrystalline nanoparticles produced from a face-centered cubic crystal and amorphous nanoparticles were prepared. Crystalline nanoparticles possess crystal facets, steps, and sharp edges on their surfaces, while amorphous nanoparticles have comparatively smooth surfaces, although some atomic roughness still remains. We have compared our numerical results with macroscopic counterparts described by Hertzian contact theory.

For monocrystalline nanoparticles, two different contact types, a facet contact and an edge contact, arising from the surface geometry of the faceted nanoparticles were taken into account. The impact on the facets causes dynamic properties to deviate considerably from predictions of the Hertz contact theory. The collision on facets of both particles reveals a non-Hertzian contact force  $F_N \propto \delta^n$ , where  $\delta$  denotes the overlap and  $n < 3/2$  when the nanoparticles are sufficiently compressed. The mutual contact surface area of the colliding nanoparticles does not expand in the quasi-elastic collision regime.

In contrast, during the edge collision, the mutual contact surface area expands, as opposed to the facet collision case. The impact force for the edge collision shows excellent quantitative agreement with the Hertzian contact force when compression is sufficiently high,  $\delta/R > 10^{-2}$ .

For a system in which orientation of the nanoparticles cannot be controlled, the possibility of precise facet contact is not high. Overall collisional behavior of the nanoparticles is thought to be dominated by edge contact; hence, Hertzian contact theory is valid in this regard. However, a crystallographic orientation-controlled system, for instance the oriented attachment technique [37], may have to consider the non-Hertzian interactions we have demonstrated, if nanoparticles are compelled to impact on facets together.

In addition to the crystalline nanoparticle case, collisions of amorphous nanoparticles, which have a rather spherical shape, were simulated in the same manner to examine the influence of facet-free surface structure. The impact force of amorphous nanoparticles agrees qualitatively,  $F_N \propto \delta^n$ , where  $n \approx 1.5$ . However, a dynamic effect on the impact force is observed.

In both crystalline and amorphous nanoparticles, a departure from the Hertzian contact force is commonly seen when nanoparticles are weakly compressed,  $\delta/R < 10^{-2}$ . In this compression regime, we found that only a few atoms on each contact surface are involved in contact and surface discreteness influences the impact force.

## Acknowledgments

We thank the U.S. Army Research Office for partial support of the present research.

## References

## References

- [1] B. Luan, M. O. Robbins, The breakdown of continuum models for mechanical contacts, *Nature* 435 (7044) (2005) 929–932.
- [2] H. Hertz, On the contact of elastic solids, *J. Reine Angew. Math.* 92 (1881) 156–171.
- [3] L. Pastewka, M. O. Robbins, Contact area of rough spheres: Large scale simulations and simple scaling laws, *Applied Phys. Lett.* 108 (22).
- [4] A. S. Barnard, N. P. Young, A. I. Kirkland, M. A. Van Huis, H. Xu, Nanogold: a quantitative phase map, *ACS Nano* 3 (6) (2009) 1431–1436.
- [5] C. Dominik, A. G. G. M. Tielens, Resistance to sliding on atomic scales in the adhesive contact of two elastic spheres, *Philos. Mag. A* 73 (5) (1996) 1279–1302.
- [6] A. Awasthi, S. C. Hendy, P. Zoontjens, S. A. Brown, F. Natali, Molecular dynamics simulations of reflection and adhesion behavior in lennard-jones cluster deposition, *Phys. Rev. B* 76 (11) 115437.
- [7] S. Luding, H. J. Herrmann, Cluster-growth in freely cooling granular media, *Chaos* 9 (3).
- [8] J. Xu, B. Zheng, Y. Liu, Solitary wave in one-dimensional buckyball system at nanoscale, *Scientific Reports* 6 (2016) 21052 EP –.
- [9] V. F. Nesterenko, Propagation of nonlinear compression pulses in granular media, *J. Appl. Mech. Tech. Phys.* 24 (5) (1983) 733–43.
- [10] V. Nesterenko, *Dynamics of Heterogeneous Materials*, Springer, 2001.
- [11] S. Sen, J. Hong, J. Bang, E. Avalos, R. Doney, Solitary waves in the granular chain, *Physics Reports* 462 (2) (2008) 21 – 66.
- [12] H. Kuninaka, H. Hayakawa, Super-elastic collisions in a thermally activated system, *Prog. Theor. Phys. Suppl.* 178 (2009) 157–162.

- [13] Q. Zeng, A. Yu, G. Lu, Evaluation of interaction forces between nanoparticles by molecular dynamics simulation, *Ind. Eng. Chem. Res.* 49 (24) (2010) 12793–12797.
- [14] H. Kuninaka, H. Hayakawa, Simulation of cohesive head-on collisions of thermally activated nanoclusters, *Phys. Rev. E* 79 (2009) 031309.
- [15] L. B. Han, Q. An, S. N. Luo, W. A. Goddard III, Ultra-elastic and inelastic impact of cu nanoparticles, *Mater. Lett.* 64 (20) (2010) 2230–2232.
- [16] Y. Takato, S. Sen, J. B. Lechman, Strong plastic deformation and softening of fast colliding nanoparticles, *Phys. Rev. E* 89 (3) (2014) 033308.
- [17] Y. Takato, M. E. Benson, S. Sen, Rich collision dynamics of soft and sticky crystalline nanoparticles: Numerical experiments, *Phys. Rev. E* 92 (2015) 032403.
- [18] C. Thornton, Z. Ning, A theoretical model for the stick/bounce behaviour of adhesive, elastic-plastic spheres, *Powder technol.* 99 (2) (1998) 154–162.
- [19] A. Awasthi, S. C. Hendy, P. Zoontjens, S. A. Brown, Reentrant adhesion behavior in nanocluster deposition, *Phys. Rev. Lett.* 97 (18) (2006) 186103.
- [20] S.-c. Jung, D. Suh, W.-s. Yoon, Molecular dynamics simulation on the energy exchanges and adhesion probability of a nano-sized particle colliding with a weakly attractive static surface, *J. Aerosol Sci.* 41 (8) (2010) 745–759.
- [21] J. D. Weeks, D. Chandler, H. C. Andersen, Role of repulsive forces in determining the equilibrium structure of simple liquids, *J. Chem. Phys.* 54 (12) (1971) 5237–5247.
- [22] K. Johnson, *Contact Mechanics*, Cambridge University Press, 1987.
- [23] D. Sun, C. Daraio, S. Sen, Nonlinear repulsive force between two solids with axial symmetry, *Phys. Rev. E* 83 (2011) 066605.
- [24] W. D. Kristensen, Computer-simulated amorphous structures (i). quenching of a lennard-jones model system, *J. Non-Cryst. Solids* 21 (3) (1976) 303–318.
- [25] S. Nosé, F. Yonezawa, Isobaric-isothermal molecular dynamics study on the glass transition of a lennard-jones system, *Solid State Commun.* 56 (12) (1985) 1005–1008.
- [26] A. Rahman, M. Mandell, J. McTague, Molecular dynamics study of an amorphous lennard-jones system at low temperature, *J. Chem. Phys.* 64 (4) (1976) 1564–1568.
- [27] S. Plimpton, Fast parallel algorithms for short-range molecular dynamics, *J. Comput. Phys.* 117 (1) (1995) 1 – 19.
- [28] W. Humphrey, A. Dalke, K. Schulten, Vmd - visual molecular dynamics, *J. Molec. Graphics* 14 (1996) 33 – 38.
- [29] S. Kim, Elastic behavior of spherical nanodroplets in head-on collisions, *J. Korean Phys. Soc.* 56 (2010) 969–972.
- [30] M. Vergeles, A. Maritan, J. Koplik, J. R. Banavar, Adhesion of solids, *Phys. Rev. E* 56 (3) (1997) 2626.
- [31] M. Y. Yi, D. S. Kim, J. W. Lee, J. Koplik, Molecular dynamics (md) simulation on the collision of a nano-sized particle onto another nano-sized particle adhered on a flat substrate, *J. Aerosol Sci.* 36 (12) (2005) 1427–1443.
- [32] P. Valentini, T. Dumitrică, Microscopic theory for nanoparticle-surface collisions in crystalline silicon, *Phys. Rev. B* 75 (22) (2007) 224106.
- [33] S.-C. Jung, J.-G. Bang, W.-s. Yoon, Applicability of the macro-scale elastic contact theories for the prediction of nano-scaled particle collision with a rigid flat surface under non-adhesive and weakly-adhesive conditions, *J. Aerosol Sci.* 50 (2012) 26–37.
- [34] K. Johnson, K. Kendall, A. Roberts, Surface energy and the contact of elastic solids, *Proc. R. Soc. Lond. A, Math. Phys. Sci.* 324 (1558) (1971) 301–313.
- [35] J.-J. Bian, G.-F. Wang, Atomistic deformation mechanisms in copper nanoparticles, *Journal of Computational and Theoretical Nanoscience* 10 (9) (2013) 2299–2303.
- [36] M. Baskes, Modified embedded-atom potentials for cubic materials and impurities, *Phys. Rev. B* 46 (5) (1992) 2727.
- [37] A. Halder, N. Ravishankar, Ultrafine single-crystalline gold nanowire arrays by oriented attachment, *Adv. Mater.* 19 (14) (2007) 1854–1858.